Featured Article

Modeling and Simulation of Hepatic Drug Disposition Using a Physiologically Based, Multi-agent In Silico Liver

Li Yan,[1] Glen E. P. Ropella,[2] Sunwoo Park,[2] Michael S. Roberts,[3] and C. Anthony Hunt[1,2,4]

Purpose. Validate a physiologically based, mechanistic, in silico liver (ISL) for studying the hepatic disposition and metabolism of antipyrine, atenolol, labetalol, diltiazem, and sucrose administered alone or in combination.

Materials and Methods. Autonomous software objects representing hepatic components such as metabolic enzymes, cells, and microarchitectural details were plugged together to form a functioning liver analogue. Microarchitecture features were represented separately from drug metabolizing functions. Each ISL component interacts uniquely with mobile objects. Outflow profiles were recorded and compared to wet-lab data. A single ISL structure was selected, parameterized, and held constant for all compounds. Parameters sensitive to drug-specific physicochemical properties were tuned so that ISL outflow profiles matched *in situ* outflow profiles.

Results. ISL simulations were validated separately and together against *in situ* data and prior physiologically based pharmacokinetic (PBPK) predictions. The consequences of ISL parameter changes on outflow profiles were explored. Selected changes altered outflow profiles in ways consistent with knowledge of hepatic anatomy and physiology and drug physicochemical properties.

Conclusions. A synthetic, agent-oriented in silico liver has been developed and successfully validated, enabling us to posit that static and dynamic ISL mechanistic details, although abstract, map realistically to hepatic mechanistic details in PBPK simulations.

KEY WORDS: agent-based; complex systems; discrete event; liver; mechanistic; modeling; physiologically based; predict; simulation.

INTRODUCTION

The vision of physiologically based (PB) pharmacokinetic (PK) modeling (1) is to provide a mechanistic and more realistic description of the behavior of substances in various tissues, with the intent of addressing such questions as: "Why do we see the observed behavior? Can we explain differences among compounds?" How do we better anticipate pharmacokinetics in patients, when a compound is administered alone or with other drugs "from *in vitro* and preclinical information?" How can we "provide increasingly confident predictions of events occurring with drugs at target and other sites ... with age, in disease?" For that vision to be achieved, we need "realistic yet more complex models that take into account such factors as the various physical spaces within tissues, the existence of permeability barriers, organ heterogeneity, and active transport or metabolic processes," (1) all within a reliable and easily reused simulation framework. Progress has not yet been sufficient to enable answering these questions today. Consequently, expediting achievement of that vision was a factor motivating development of the recently described in silico liver (ISL) (2). It is an example of a (new) class of synthetic, discrete, componentized, physiologically based, computational, analogue models that are intended for refining, exploring, and testing hypotheses about interacting mechanisms that influence the transport, metabolism, and hepatic disposition of compounds of interest. It is intended for unraveling the complexity of the interacting features of hepatic disposition defined by *simulation* of events occurring within the PBPK context, but using a precise representation of the hepatic architecture, biochemistry and physiology. In contrast, classical PBPK models, as exemplified in (3–8), make parsimony paramount. By emphasizing

[1] The UCSF/UCB Joint Graduate Group in Bioengineering, University of California, Berkeley California 94720, USA.

[2] Department of Biopharmaceutical Sciences, University of California, 513 Parnassus Ave., S-926, San Francisco California 94143-0446, USA.

[3] School of Medicine, Princess Alexandra Hospital, University of Queensland, Woolloongabba, Queensland 4102, Australia.

[4] To whom correspondence should be addressed. (e-mail: a.hunt@ ucsf.edu)

ABBREVIATIONS: CV, central vein; ISL(s), in silico liver(s); MW, molecular weight; PB, physiologically based; PCPs, physicochemical properties; PK, pharmacokinetic; PV, portal vein; S_1 and S_2, two classes of SSs; SD, standard deviation; SS(s), sinusoidal segment(s).

identifiability and certainty of parameters obtained by nonlinear regression, they emphasize describing PK data in terms of the simplest global representation of physiological events. Once that has been done satisfactorily, interest turns logically to the problem of gaining a better understanding of the detailed mechanisms underlying the data. Historically, the only practical approach was to adapt analytical modeling methods and use equations to represent posited mechanistic details. Traditional PBPK models are an example of that approach. The approach, however, encounters obstacles when there is incomplete knowledge about the mechanistic details. Coincident with advances in object-oriented programming, it became feasible to focus directly on mechanisms by asking, what mechanisms can I build from software components (objects) that when measured in some way will yield data comparable to my referent data? The model that results from such building and validation is not inductive: it is synthetic.

Other key features of the similarities and differences between traditional, induced, PK models and synthetic models of the ISL type have been detailed under Supplementary Material ESM in (2) and in (9) and (10). It becomes clear that the two model classes have different goals and uses. If future ISL models become more predictive, it will be because they are more realistic and thus more complicated. In contrast, PBPK models defined using nonlinear regression tend to be more robust because the fewest number of parameters possible are used, recognizing that for induced, mathematical models, each additional parameter adds to model uncertainty and may compromise predictive power. For models of the ISL class, the following has been a working hypothesis. Through the combined use of discrete and synthetic methods to more realistically represent underlying 3D morphology and microevents, computational scientists will be able to better predict the PK consequence of changes in drug structure or pathology, for example, by using validated simulations like the ISL, as distinct from the more conventional PBPK regression approaches. Although this report is an important step toward that end, further research will be needed to support that working hypothesis.

Within this first generation of ISL, hepatic form and function are disjoined: different, autonomous components represent them separately at several levels. This disjunction does not occur in reality and that issue will be addressed in later ISL generations. Computational efficiency in this first generation is facilitated by having aspects of hepatic microarchitecture represented independently by components (the agents and functional objects described under "MATERIALS AND METHODS"), rather than equations, arranged to represent spatial organization of function. Further, each ISL component can interact uniquely with mobile objects representing drugs and other compounds of interest. Indeed, a variety of different mobile objects can be studied, simultaneously or separately. The consequences of interactions between simulated drugs and spatially confined components, controlled by known or hypothesized component-specific principles, can be measured and studied analogous to wet-lab experiments. The resulting data can be compared with (as distinct from being fit to) *in vitro* and *in situ* data to refine the ISL and help clarify posited, causal linkages thought to underlie hepatic disposition phenomena.

Research on this class of models is motivated by achieving three broad goals. 1) Experimentation with such models will help unravel complex pharmacokinetic processes. 2) Future device components can be reused and "educated," for example, as in (1) and (11), to use the physicochemical properties (PCPs) of new compounds as input to generate expected hepatic disposition data that can be mapped to the species of interest. 3) With progress on 1) and 2), expected hepatic disposition and drug metabolism properties for sets of new compounds can be explored in advance of costly wet-lab experiments or clinical trials, potentially saving considerable time. Achieving these capabilities will require pushing modeling and simulation capabilities such that we can methodically capture more multi-scale knowledge within models.

To what extent can different ISLs overcome limitations encountered by traditional PBPK models? Exactly what is needed to move toward the above expectations? Hunt *et al.* (2) suggested that the following may be possible. 1) Having specified an ISL, separately parameterize and hold constant its key microarchitectural features. 2) Dose with simulated counterparts of each of several previously studied compounds. 3) Enable the ISL to distinguish among the different simulated compounds. 4) Adjust only PCP-sensitive, ISL parameters so that the in silico disposition properties of the simulated compounds—dosed alone or in combination—match the known properties of those compounds reasonably well so that a similarity criterion is met.

In this work, we apply the ISL to describe the isolated perfused rat liver systems, in an attempt to advance on traditional models that have been used to evaluate hepatic drug disposition and clearance (3–8). Recognizing that cationic drugs account for 70 to 80% of all drugs (12), we simulated the hepatic disposition and metabolism of four cationic compounds, atenolol, antipyrine, labetalol, and diltiazem, along with the co-administered, neutral extravascular marker sucrose. We verified that the ISL could generate in silico experimental results that were indistinguishable from those measured during *in situ* experiments. We followed an iterative ISL refinement procedure that led to a single core ISL structure parameterization that could be used for all five compounds. Only the parameter values of PCP-sensitive, ISL components that interact differently with different compounds were tuned to give good compound-specific results. Monte Carlo variants of the resulting ISLs were used to simulate outflow profiles for all five compounds, alone or in combination. The results provide additional ISL validation evidence.

Because of the non-deterministic nature of the ISL, the consequences of PCP-sensitive, parameter changes are neither unique nor simple. The consequences of changing four, PCP-sensitive, probabilistic parameter values are presented and discussed to illustrate specifically how a change in PCPs can be expected to alter ISL behavior. Two consider changes in the probability of simulated drug moving between sinusoidal spaces, the third reflects on changing the probability of simulated intracellular binding, and the forth deals with changing the probability of a metabolic event. Based on that validation, we hypothesize that static and dynamic ISL mechanistic details, although abstract, map realistically to hepatic mechanistic details. The results represent an important advance in the science and methods of PBPK modeling and simulation.

MATERIALS AND METHODS

To clearly distinguish in silico components and processes from corresponding hepatic structures and processes, we use SMALL CAPS when referring to the in silico counterparts.

ISL Structure and Design

ISL structure is illustrated in Figs. 1 and 2 and detailed in Hunt *et al*. (2). For convenience, an abridged description is provided along with a brief rationale for ISL component design. Where most useful, we contrast the ISL with conventional PK models. See (2) and its Supplemental Material ESM, along with (9) and (10) for additional discussion of design considerations and contrasts. The ISL is an abstract, physiologically based representation of a hepatic lobule. It is not intended to duplicate a liver, detail-for-detail. An operating guideline has been that if results of in silico experiments reasonably match wet-lab counterparts over a variety of experiments, then the in silico mechanistic details may map to corresponding *in vivo* or *in situ* details in

Fig. 2. Illustrations of two key ISL components. **A** A schematic of a sinusoidal segment (*SS*): one SS occupies each node specified by the directed graph (Fig. 3). Grids represent spaces and can contain objects representing the functions associated with a portion of sinusoids. Objects representing DRUG and SUCROSE enter and exit via the Core and Grid A. From Grid A, they can access the other spaces. Grid locations have properties that govern their interaction with mobile COMPOUNDS. Different shadings of Grid A illustrate the potential for representing heterogeneous properties. Objects functioning as containers (for other objects) are used to represent cells, and can be assigned to any grid location. The Core represents blood flow; Grid A (referred to as Rim Space) represents the sinusoid rim; Grid B (referred to as the Endothelial Layer) represents endothelial cells and fenestra; Grid C (referred to as the Space of Disse and Hepatocyte Layer) represents all other spaces, including hepatocytes. **B** A HEPATOCYTE container: objects representing all needed intracellular components can be placed within. Only two types of intracellular BINDERS recognize drug: those that simply bind (*b*) and those that represent enzymes (*e*) and can metabolize. Cell containers will not allow SUCROSE to enter. Bile was not needed for these simulations but can easily be represented as a extension as described in (2).
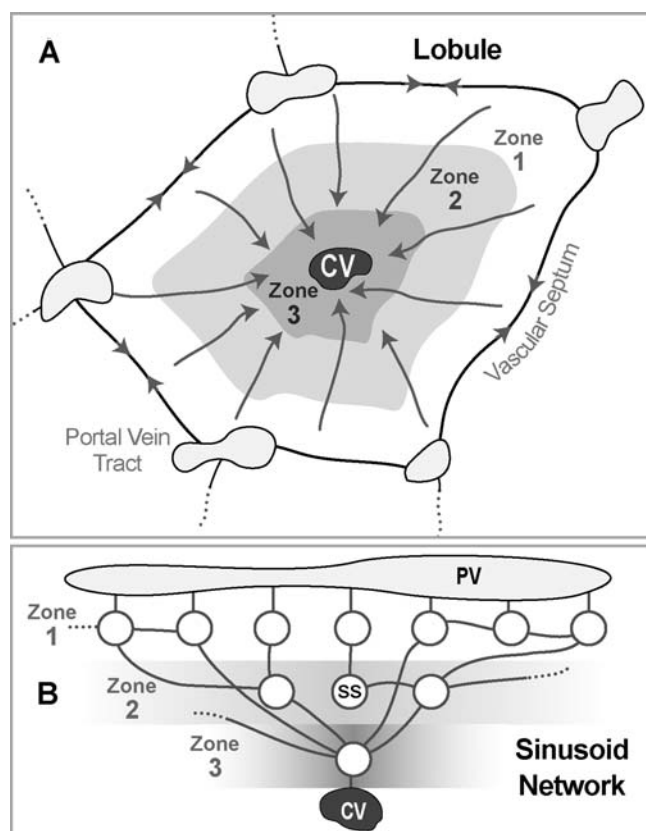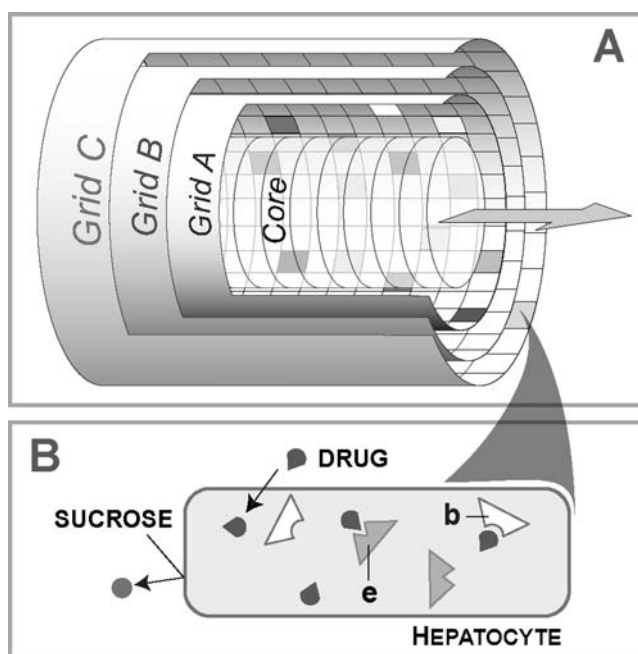

Fig. 1. Illustrations of hepatic lobular structures and their representation within the ISL. **A** A schematic of a cross-section of a hepatic lobule showing the direction of flow from the terminal protal vein tracts (*PV*) through sinusoids in three concentric zones to the central hepatic vein (*CV*). Different zones have quantitative differences in structural characteristics and enzyme levels. **B** A portion of the sinusoid network is represented by an interconnected, three zone, directed graph. Data from the literature are used to constrain the graph size and structure. *SS* Sinusoidal segment.

informative ways. ISL components mimic essential form and function features of the *in situ* perfused rat liver system (13) used to study the hepatic disposition of sucrose, antipyrine, atenolol, labetalol, and diltiazem, the compounds on which this report focuses. In (5), the portal vein was cannulated to enable single pass perfusion; perfusate was collected using a fraction collector. The fraction of the administered dose contained per unit of collected perfusate was measured. ISL experiments follow the same protocol (5).

The liver is composed of secondary units, which are composed of several lobules. We assume that lobules are similar throughout the liver and within secondary units. Our task thus reduces to simulating a large collection of lobules. Blood flows through the lobules via sinusoids, which provide access to hepatocytes. Blood enters lobules through portal vein tracts (PV) and vascular septa, and drains into branches of a common central vein (CV) (14). The acinar flow patterns

within a lobule are represented in the ISL by a directed graph (Fig. 1), which abstractly mimics these flow paths. To illustrate, a flow path from PV to CV can be divided into three segments and represented by a directed graph: PV to node 1, node 1 to node 2, and node 2 to CV. Following that method, hepatic function is represented within the segments. ISL graph edges represent flow connections between the graph nodes, called Sinusoidal Segments (SSs). Because traditional PK models have focused primarily on the PK data and its structure, information about paths and their interconnections has been abstracted away. Such abstractions are adequate when the primary use is systemic prediction for which those details are not needed.

Representing Sinusoidal Details

The usage and aspect focus taken on hepatic sinusoidal function dictates the simplest 3D ISL component representation for a SS. Our primary use has been to match current and future hepatic outflow profiles for many drugs using just one, basic ISL structure. The interesting aspects are those that interact with administered compounds moving through sinusoids. Starting simple, we used exploratory modeling protocols to assess the suitability of a variety of component structures. The first effective structure is shown in Fig. 2A. A SS represents a unit of sinusoid function, along with its related spatial features. The design and construction validates against the considerable body of qualitative, histological data available in the literature. A SS is a discretized, tube-like structure comprised of a blood "Core" surrounded by three identically sized 2D grids, which together constitute a 3D structure. A more realistic 3D grid is not yet justified and tracking and managing events occurring in concentric 2D grids is computationally simpler than in 3D grids.

Grid A represents sinusoid edges near endothelial cells. Grid B is wrapped around Grid A to represent the endothelial layer. The parameter *ECDensity* controls the size and prevalence of FENETRATIONS within Grid B: in this report, 20% is randomly assigned to FENESTRA, and the remaining space is assigned to CELLS. Grid C is wrapped around Grid B; it represents the Space of Dissé and hepatocytes. They are separate in the liver. Here we represent the Space of Dissé and hepatocytes using one, rather than two spaces. Two can be used. However, during the exploratory modeling referred to above, it became clear that conflating their representation into one space, one grid, would provide model detail that was adequate to achieve project goals. The parameter *HepDensity* controls the relative fraction of Grid C assigned to HEPATOCYTES. We specify two SS classes: S_1 and S_2. Compared to a S_2, a S_1 has a shorter internal path length and a smaller surface-to-volume ratio. We found that it was essential to have sufficient variety of effective SS lengths and diameters. There are several ways to provide that variety. Using two classes of SS was the first strategy that was successful. The merits of alternative, possibly simpler strategies are being explored. As described in Table S1, SS length is given by a random draw from a modified gamma distribution having a parameter-specified mean and variance. We used that distribution because drawing from a uniform distribution failed. The same proved true for normal and unmodified gamma distributions.

Interconnecting Sinusoids

The blood supply for one lobule feeds into several sinusoids that merge in stages to only a small fraction of their original number as blood is fed into the lobule's outgoing CV. Interconnections between sinusoids are frequent in the periportal region but are not seen near the CV. The ISL's graph structure reflects that arrangement. Miller *et al.* (15) and Gumucio *et al.* (16) subdivide the lobule interior into three concentric zones to distinguish the quantitative difference in structural characteristics and enzyme levels among different zones. Figure 1 illustrates that we do the same. The resulting directed graph maps to a portion of a lobule's sinusoidal network and to half an acinus. In the ISL, each zone contains at least one node. There are three graph structure parameters: 1) number of nodes, 2) number of intra-zone connections, and 3) number of inter-zone connections. Graph connectivity (assignment of edges to nodes) is randomly specified for each simulation to emulate intra-hepatic lobule variability and uncertainty about sinusoidal fine structure. Consequently, each is unique. The number of nodes per zone is always in the order Zone 1 > Zone 2 > Zone 3. As specified in Table I, there are more interconnections between Zone 1 nodes than between Zone 2 nodes. There are no interconnections between Zone 3 nodes. Figure 3 shows an example of a LOBULE graph structure that was used for one simulation run. In (2), we used available literature observations to narrow the variety and range of stochastically allowed graph structures.

For the intended uses, the ISL has what we believe is a minimum set of hepatic features. It is designed to enable new features and functions to be easily added (or removed) without interfering with the function of the existing components and features. It is designed to be reused. Structural and spatial parameterizations that have been validated for one set of drugs can be held constant while drug-specific parameters are tuned to match data for additional sets of drugs.

Compounds as Unique Objects

ISL parameters are grouped into three categories: 1) those that control LOBULE graph and 2) sinusoid structures, and 3) those that reflect the influence of the physicochemical properties (PCPs) of mobile compounds. For convenience, the parameters in the latter are segregated into three groups: those for which compound's (a) molecular weight (MW) and size, (b) partition coefficient ($\log P_{app}$), and (c) unbound fraction are thought to exert a strong influence. Table I lists the ISL parameter names, descriptions, and values. Additional detail is available in Supplementary Material.

The COMPOUNDS studied are in silico analogues of sucrose, a neutral extracellular space maker, and four cationic drugs: antipyrine, atenolol, labetalol, and diltiazem. The wet-lab outflow profiles against which simulations have been validated are reported in (5). Each compound is represented using objects that move through the LOBULE and interact with each SS feature encountered. A typical COMPOUND represents many drug molecules: the value and the mapping to wetlab data is controlled by the parameter *ISL2WetLabScaling*. A COMPOUND'S behavior is determined by the PCPs of its referent, along with the LOBULE and SS features encountered

Table I. ISL Parameters, Descriptions, and Values

Category	Name	Description	Value[a]
Lobule Graph	GraphSpecFile	Node in Zone I	45
		Node in Zone 2	21
		Node in Zone 3	6
		Intra-Zone I edges	18
		Intra-Zone II edges	10
		Intra-Zone III edges	0
		Zone I → Zone II edges	15
		Zone I → Zone III edges	0
		Zone II → Zone III edges	8
Sinusoid Structure Parameters	*DirSinRatio*	Percentage of SS that are type S_1 (direct)	0.75
	TortSinRatio	Percentage of SS that are type S_2 (tortuous)	0.25
	DirSinCircMin	Upper and lower bounds of the SS circumference, generated by a pseudo-random number using the uniform distribution	50
	DirSinCircMax		50
	TortSinCircMin		4
	TortSinCircMax		4
	DirSinLenAlpha	Length of SS, generated by a modified Gamma distribution; the modification consists of a leftright shift of the distribution, allowing the user to clip off the front of the distribution	3.0
	DirSinLenBeta		0.215
	DirSinLenShift		0
	TortSinLenAlpha		10
	TortSinLenBeta		0.125
	TortSinLenShift		−40
	ECDensity	Relative ENDOTHELIAL CELL density within Grid B	0.8
	HepDensity	Relative HEPATOCYTES density within Grid C	0.6
Parameters influenced by MW	*SinusoidTurbo*	The complement of the amount of turbulence allowed in SS	0.3
	CoreFlowRate	The number spaces moved forward within the SS core during each step	2
	ISL2WetLabScaling[b]	Provides the precise validation mapping from ISL output to the wet-lab (IPRL) output fraction	7
Parameters influenced by $\log P_{app}$	*A2BJumpProb*	Probability that a COMPOUND will jump from Grid A to Grid B when given the option	0.1
	B2AJumpProb	As above: from Grid B to Grid A	0.6
	B2CJumpProb	As above: from Grid B to Grid C	0.35
	C2BJumpProb	As above: from Grid C to Grid B	0.65
Parameters influenced by protein binding	*BindersPerCellMin*	Min and max for the number of binding agents inside each CELL.	5
	BindersPerCellMax	Simple BINDERS for ECS and ENZYMES for HEPATOCYTES.	10
	MetabolizeProb	Probability that an ENZYME will metabolize a SOLUTE	0.4
	SoluteBindingProb	Probability a SOLUTE will be bound when contact a BINDER	0.5
	SoluteBindingCycle	Number of cycles a BINDER will bind a SOLUTE	25

[a] Parameter values when SUCROSE and ANTIPYRINE were dosed in combination.
[b] In (2), *ISL2WetLabScaling* is called *SoluteScale*.

during its unique trek from PV to CV. During a simulation cycle, an encountered component "reads" the information carried by a COMPOUND and then uses it to customize its response, in compliance with its parameter values, following some pre-specified or learned logic (11). For example, a CELL detects a COMPOUND in an adjacent space and "reads" that $P_{app}=0$ (because it is SUCROSE). It therefore does not allow that object to enter. The dosage function simulates the effects of catheters and large vessels; Hung *et al.* (5) used an inverse Gaussian function for this purpose; we used a modified gamma function.

COMPOUNDS enter the lobule via the PV. After that, they enter a SS in Zone 1 at either the Core or Grid A. Simulated flow occurs only in the Core. The parameter *SinusoidTurbo*, which represents flow turbulence, biases COMPOUND movement in the three spaces in the CV direction. Until being collected at the CV, each COMPOUND has several stochastic options. In the Core or Grid A, a COMPOUND can move within either space, jump to an adjacent space, or exit the SS. Within Grid B, it has three options: move within that space, jump back to the Grid A, or on to Grid C. All COMPOUNDS can move within the EXTRACELLULAR portions of Grids B and C. A DRUG but not SUCROSE can move into CELLS in either Grid B or C. A COMPOUND can exit a SS only from Grid A or the Core. After a COMPOUND exits a SS in Zone 3, it enters the CV: its arrival is recorded, simulating being collected by a fraction collector.
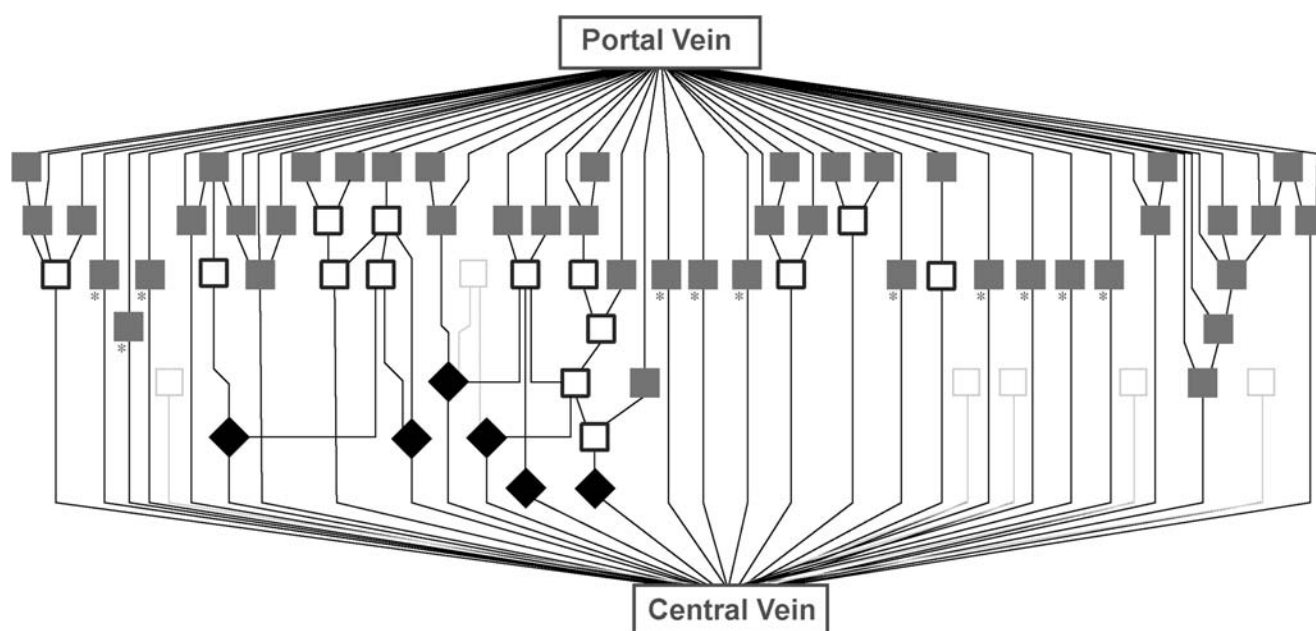
Fig. 3. A sample ISL lobule graph structure generated for one simulation run. All Zone 1 nodes (gray squares) have one incoming edge from the PV. They have one outgoing edge; it can be connected to another SS or to the CV. Zone 2 nodes (unfilled squares) have an edge incoming from a Zone 1 SS; the outgoing edge can be connected to a SS in Zone 2 or 3. Zone 3 nodes (black diamonds) have one incoming edge from a Zone 2 SS; the outgoing edge is connected to the CV. The seven, light gray, unfilled squares represent Zone 2 nodes that, by chance, were not assigned an incoming edge. *Asterisk* As drawn, these Zone 1 nodes look identical. However, the SS placed at each such apparently identical node is different: they can be either S_1 or S_2; within both types, size and other details can be different. When needed, a parallel, mirror image graph structure can be added to represent biliary excretion.

Representing Cells and Subcellular Components

An unspecified number of cells are represented by objects (called CELLS) in Grids B and C: they function as containers for other objects. A grid location and its container are the limit of spatial resolution. At the start of each simulation, CELLS are placed randomly at some fraction of the available grid locations. A HEPATOCYTE is illustrated in Fig. 2B. In this report, each CELL contains a randomly specified number of BINDERS in a well-stirred space. No additional detail was needed for validation. The objects within CELLS are below that level, but that condition too can be easily changed when needed.

BINDERS are the INTRACELLULAR components that represent transporters, enzymes, and other cellular material that binds or sequesters drug molecules. A binder within a Grid B CELL can only bind and later release a DRUG. A binder within a Grid C HEPATOCYTE is called an ENZYME because it can bind DRUG and either release or METABOLIZE it. As done in (17) and (18), an ENZYME can be designed to bind more than one DRUG object. Additional objects or agents can be specified and added as needed without compromising either ISL function or the function of objects already present. Because of the stochastic nature of ISL simulations, each in silico experiment generates a slightly different outflow profile. Typically, a single experiment is comprised of 48 trials that were averaged to represent a referent outflow profile. Because we used an 8-node computer cluster (see below), it was convenient to run a number of experiments that was divisible by eight. Forty experiments proved to be too few and 56 were unnecessary. Results of the 48 experiments were averaged to represent a referent outflow profile.

Drug partitioning into cells was simulated as follows. If a COMPOUND is adjacent to a CELL container and all other grid points around the COMPOUND are empty, then (when *SinusoidTurbo*=0) there is an equal probability of it moving in any of the available directions. There is a 1-in-11 chance that it will try to move to the CELL'S location. If the solute decides to move to that location and the parameter *isMembraneCrossing* is true, because $P_{app} \neq 0$, then the COMPOUND enters the CELL. As more COMPOUNDS are successfully simulated using future ISLs, we expect to assign a probability to CELL entry when *isMembraneCrossing* is true.

Similarity Measure

Due to differences between rats and among experimental details, no two liver perfusion outflow profiles are identical. Assuming that experimental, quality control measures are met, there are no specific metrics for deciding when the next *in situ* outflow profile is sufficiently similar to those already completed to be classified as a repeat experiment. Typically, the decision is made by the researcher based on inspection of the data, guided by experience. Ideally, an ISL outflow profile should be indistinguishable from the wet-lab profile of an acceptable repeat experiment, as judged by an expert (this characteristic is one of ten, targeted ISL design capabilities listed in Supplementary Material ESM). Whereas the precision simulation output of an inductive, mathematical model can be precisely fit to certain selected referent data, the output of an ISL experiment cannot, because it mimics the referent, *in situ* experiments, where results vary among repeat experiments. It can, however, be quantitatively compared. We

attempted to capture key features of expert opinion in a quantitative Similarity Measure (SM). It compares in silico with the referent outflow profiles as detailed in (2). Briefly, we assumed that the coefficients of variation of repeat observations (referent) are constant. For each referent outflow profile measure P, we create two curves, $P^l = P(1-d)$ and $P^u = P(1+d)$. They were the lower and upper bounds of a band around P. Here, d is the standard deviation of the relative differences between each of six replicate *in situ* experiments and the mean value for a given collection interval, pooled over all collection intervals. An ISL outflow profile was deemed similar to the referent if 80% or more of ISL outflow values were within the band (SM ≥ 0.8).

Parameter Tuning

There are thirty-seven ISL parameters. Several represent hepatic structures that are not influenced by the PCPs of a referent compound. A major simulation task has been to locate a region of ISL parameter space that can provide parameter vectors that generate biologically realistic outflow profiles that meet the SM criteria for sucrose and the co-administered referent drug. Because SUCROSE is a marker for accessible extracellular spaces, we focused on it first. We tuned the LOBULE graph and SS structure parameter values so that the referent sucrose outflow profiles met the minimum SM value. We then held those values constant and focused on antipyrine, the least lipophilic of the four drugs. We assumed that when co-injected, the initial appearance of sucrose and antipyrine would be similar (within 1 second of each other). When needed, a small lag-time was used to make that adjustment for each of the referent drugs. We tuned the PCP-sensitive parameters, including parameterizations of all intracellular objects, to improve SM values. We then continued the iterative tuning process to obtain a single ISL from which acceptable outflow profiles would be obtained following administration of any combination of SUCROSE, ATENOLOL, ANTIPYRINE, LABETALOL, and DILTIAZEM.

Consequences of Parameter Changes

In most cases, a change in an outflow profile caused by altering the value of one parameter can be compensated by adjusting a small set of other parameter values. As part of the verification process, it was important to demonstrate that a change in a COMPOUND'S parameter value produced the type of outflow profile alteration that would be expected based on knowledge of hepatic anatomy and drug disposition. With that in mind, we undertook a series of experiments that focused on four, PCP-sensitive, ISL parameters, two that control a COMPOUND'S stochastic movement between grid spaces and the two that control INTRACELLULAR binding and METABOLISM. A change in any of these four values could map to a relative change in a specific hepatic feature resulting from different genetics, differences between individuals, or the consequences of certain hepatic diseases; or it could map to differences in PCPs.

The parameter *A2BJumpProb* specifies the probability that, within each simulation cycle, a COMPOUND will jump from Grid A to Grid B, simulating moving from the sinusoid edge to the endothelial surface. When its value is smaller, the COMPOUND spends less time in Grids B and C, and is more likely to reach the CV sooner. A decrease in *A2BJumpProb* might be expected to map to increased binding to red cells or an increase in the fraction ionized, for example. *B2CJumpProb* specifies the probability that a COMPOUND will jump from Grid B to Grid C, simulating moving from the endothelial layer to the space of Dissé and hepatocytes. When its value is large, more compounds will move to Grid C. The net result will be that COMPOUNDS tend to spend relatively more time wandering around within Grid C. A larger value might be expected to map to an increased P_{app}, for example. The parameter *SoluteBindingProb* specifies the probability that, within each simulation cycle, an unoccupied BINDER within a CELL will bind a free COMPOUND within that same CELL. A smaller value might be expected to map to a decrease in the fraction of drug that is ionized, for example, or to fewer hydrogen bond donor groups. The parameter *MetabolizeProb* specifies the probability that a bound COMPOUND within HEPATOCYTE will METABOLIZE it rather than simply releasing it. Consider a COMPOUND that is bound to a binder object at the start of a simulation cycle (t_1) and remains bound at the end of that simulation cycle (t_2). Because simulation events within the simulation cycle are not resolved, that scenario can represent several referent scenarios, including a drug being bound to one cell component at t_1, becoming free, and then being bound by another cell component at t_2. A larger value for another drug might be expected to map to increased enzyme affinity, for example, or increased relative abundance of the specific enzyme responsible for metabolism.

Hardware

The experiments were executed on an eight-node OSCAR cluster (oscar.openclustergroup.org/) running Red-Hat's Fedora 5. The distribution of the runs uses MPICH 1.2.7 (www-unix.mcs.anl.gov/mpi/mpich1/). The ISL was compiled using GCC 4.1.1 against the Swarm 2.2.3 Objective-C libraries (swarm.org/wiki/Main_Page). Each experiment consisted of 48 Monte-Carlo runs with the initial pseudo-random number seed extracted from the machine's clock. The fraction of dose flowing out of the LOBULE was averaged over all runs. The Smodulus_smoothing function from the Rwave (version 1.22) package for R was used to smooth post-peak data using a wavelet window of two or three observations.

RESULTS

Outflow Profiles for Four Cationic Drugs plus Sucrose

In the following experiments, DRUGS are always co-administered with the same amount of SUCROSE. Following are the parameterization processes. Table II lists PCPs. The profile change induced by a modest change in one of the parameters can be reasonably compensated by adjustments in one or more of the other parameters. Increasing *A2BJumpProb* (Grid A→B) or decreasing *B2AJumpProb* (Grid B→A), for example, can reduce the peak height of an outflow profile, because more COMPOUNDS stay in Grid B: the rate of return of COMPOUNDS to Grid A and Core are reduced. Such change has been used to guide parameter tuning.

Table II. DRUG-Specific ISL Parameter Values

Category	Parameter	Atenolol	Antipyrine	Labetalol	Diltiazem
Parameters influenced by MW	*CoreFlowRate*	2	2	2	2
	ISL2WetLabScaling	7[a]	7	6	1
Parameters influenced by logP_{app}	*A2BJumpProb*	0.1	0.1	0.35	0.9
	B2AJumpProb	0.6	0.6	0.2	0.2[b]
	B2CJumpProb	0.3	0.35	0.5	0.5
	C2BJumpProb	0.6	0.65	0.5	0.2
Parameters influenced by fraction unbound	*BindersPerCellMin*	5	5	5	10
	BindersPerCellMax	10	10	10	20
	MetabolizeProb	0.35	0.4	0.3	0.02
	SoluteBindingProb	0.35	0.5	0.6	0.35
	SoluteBindingCycle	25	25	25	20
SM Values		0.92	0.81	0.91	0.97
Physicochemical properties	MW	266.3	188.2	328.4	414.5
	log P_{app}^c	0.14	0.33	2.69	3.53
	fraction unbound[c]	0.74	0.60	0.52	0.28
	pK_a^c	9.60	1.45	7.40	7.70

Values are listed for the DRUG-specific ISL parameters used to generate the outflow profiles in Figs. 4 and 5. The Similarity Measure (SM) values for those profiles are listed along with the physicochemical properties of the four drugs.
[a] *ISL2WetLabScaling* for SUCROSE that was coadministered with all four DRUG.
[b] *B2AJumpProb* for SUCROSE that was coadministered with DILTIAZEM was 0.75 to compensate the difference between *ISL2WetLabScaling* values.
[c] From (5)

We tuned the parameter values for each of the four DRUGS, as described above, until minimally acceptable SM values for the DRUG and co-administrated SUCROSE were achieved (e.g., SM≥0.5). Separately, we iteratively improved the SM values for each of the DRUGS and co-administrated SUCROSE. We choose the best LOBULE parameterization for each, four total, for the next stage of improvement. Keeping each LOBULE parameterization constant, we adjusted the remaining parameters to obtain an improved SM value (SM≥0.7). We then picked one LOBULE parameterization and held it constant while iteratively searching the PCP-influenced parameter space. This iterative process resulted in the LOBULE and SS structures for all four DRUGS specified in Table I. Acceptable outflow profile matches for each of the four DRUGS along with co-administrated SUCROSE are shown in Figs. 4 and 5. The corresponding parameter values for drug-specific physicochemical parameters and SM values are listed in Table II.

Because the molecular weight of diltiazem is much larger than that of the other three drugs, we found it convenient to set its *ISL2WetLabScaling* parameter value to 1. Because ATENOLOL and ANTIPYRINE have similar molecular weights, we used *ISL2WetLabScaling*=7 for each—the value used for SUCROSE, and used *ISL2WetLabScaling*=6 for LABETALOL, which has slightly higher molecular weight compared to ATENOLOL and ANTIPYRINE.

DILTIAZEM had the lowest *MetabolizeProb* (0.02 compared to 0.3–0.4 for the other three drugs), even though diltiazem is described in the literature being a high clearance drug. Because of DILTIAZEM's large value of *A2BJumpProb* (0.9) and small value of *C2BJumpProb* (0.2), DILTIAZEM spent relatively more time in Grid C. Consequently, metabolism was extensive even though *MetabolizeProb* was low. The high *A2BJumpProb* and low *C2BJumpProb* parameter settings map to diltiazem's physicochemical property of high lipophilicity.

Consequences of Changing DRUG-Specific Parameter Values

To study how systematic changes in the values of certain PCP-sensitive parameters influenced outflow profiles, we conducted numerous experiments focused on assessing the consequences of parameter changes. We used LABETALOL as the test DRUG because its outflow profile properties were somewhat centric of the four DRUGS. All ISL structural parameter values were unchanged from values listed in Table I. In each experiment, LABETALOL was co-administrated with an equal amount of SUCROSE. For each changed parameter setting, we calculated the ratio of the area under the LABETALOL outflow curve (over 100 simulated seconds) to the area under the curve following the parameter change: this ratio provided a relative, single value measure of the consequences of the change; we refer to the value as Area Ratio.

The first set of experiments studied the four space-jump-probability parameters, *A2BJumpProb*, *B2AJumpProb*, *B2CJumpProb*, and *C2BjumpPrpb* (for LABETALOL in Fig. 4C it was 0.35, 0.2, 0.5, and 0.5, respectively). For each, we ran sets of simulations for eight parameter values ranging from 0.05 to 1.0. The results showed a consistent trend of either increased or decreased outflow profiles with increasing parameter values. Increasing *A2BJumpProb* or decreasing *B2AJumpProb* had a similar influence on LABETALOL's outflow profile: the peak decreased. Figure 6A shows results for two *A2BJumpProb* parameter values. For *A2BJumpProb*=0.05, Area Ratio=2.5, whereas for *A2BJumpProb*=0.95, Area Ratio=0.54. The results were consistent with expectations for ISL structures and functions. Increasing *A2BJumpProb* (or decreasing *B2AJumpProb*) caused more COMPOUNDS to move into (or less out of) Grid B; from there, more moved into Grid C and that enabled increased METABOLISM.

Increasing *B2CJumpProb* or decreasing *C2BJumpProb* had similar influences on LABETALOL's outflow profile: the tail end of the profile was lowered. Figure 6B shows results for
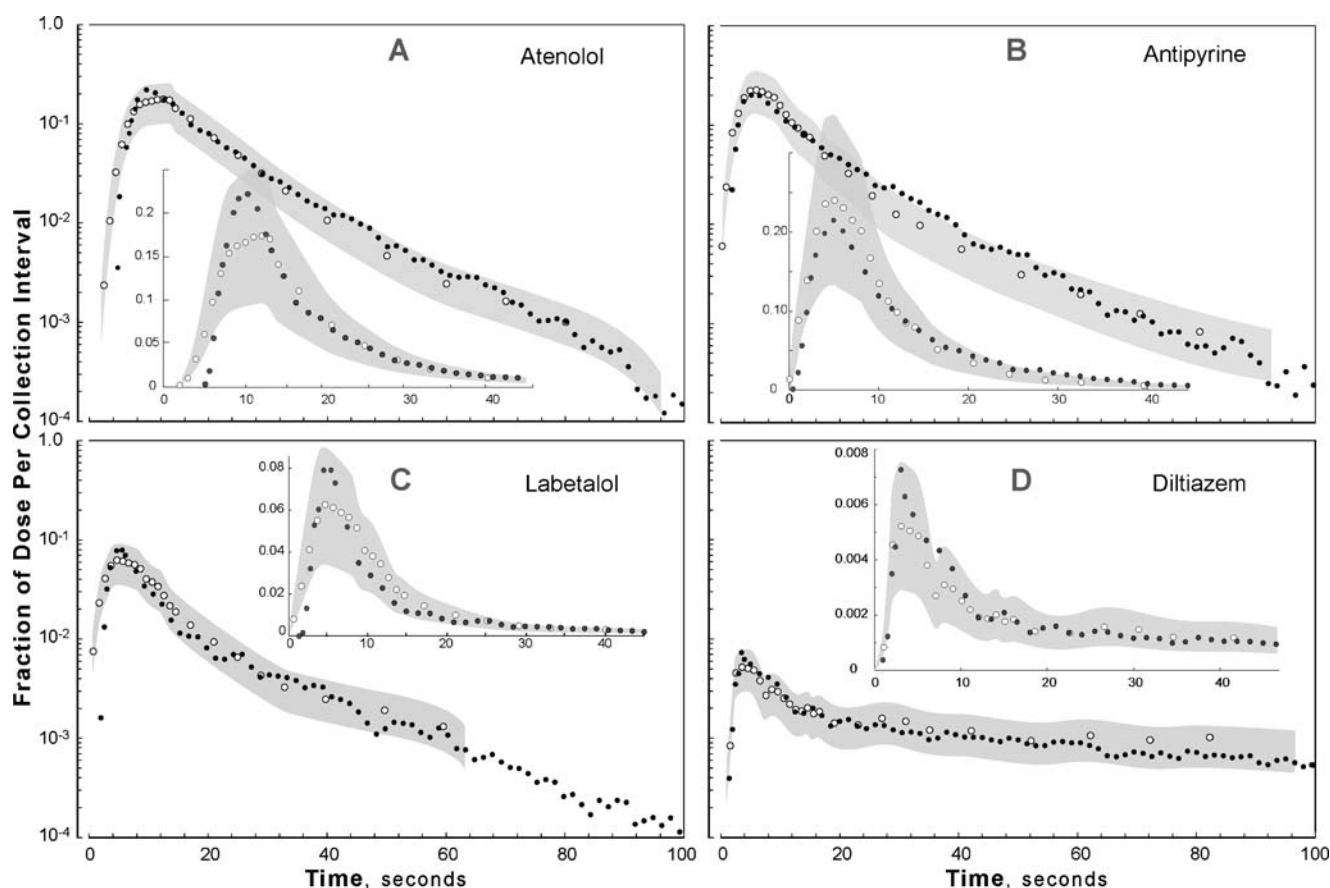
Fig. 4. Semilog and scatter plots of acceptable outflow profile matches for the four drugs. **A** ATENOLOL, **B** ANTIPYRINE, **C** LABETALOL, and **D** DILTIAZEM were co-administrated with SUCROSE. Plots show the fraction of dose per outflow unit (per ml for the referent) as a function of time (1 unit=1 second) after dosing with equal amounts of SUCROSE and DRUG. The gray band spans the range for the mean±one standard deviation as specified in the text. *Open circles* Wet-lab outflow values for each drug. *Dark gray circles* DRUG outflow values using the tuned parameter sets in Tables I and II. Each ISL datum is the smoothed (window size, three values) mean value of 48 independent ISL runs (all stochastic parameter values are changed prior to each run). Although each independent run uses the same LOBULE graph and SSs, their arrangements are randomized prior to each run; consequently, the actual structure of the LOBULE is different for each simulation. Gray band for LABETALOL ends at t=70 because the *in situ* experiment ended after 70 s. SM values: ATENOLOL, 0.92; ANTIPYRINE, 0.81; LABETALOL, 0.91; and DILTIAZEM, 0.97.

B2CJumpProb parameter values 0.05 and 0.95. Decreasing *B2CJumpProb* from 0.5 (the value for LABETALOL in Fig. 4C) to 0.05 caused the Area Ratio to increase to 1.5; increasing *C2BJumpProb* from LABETALOL'S value of 0.5 to 0.95 caused the Area Ratio to decrease to 0.83. These results were consistent with the ISL's design and hepatic histology. Increasing *B2CJumpProb* or decreasing *C2BJumpProb* increased the amount of COMPOUND in Grid C, which enabled increased METABOLISM while slowing the return of COMPOUNDS to Grid A and the Core (and thus arrival at CV). The leading edge and the peak of the outflow profile were much more sensitive to changes in *A2BJumpProb* and *B2AJumpProb* than to changes in *B2CJumpProb* and *C2BJumpProb*.

A second set of experiments explored the consequences of changing the parameter values of two CELLULAR components: *SoluteBindingProb* and *MetabolizeProb*. We again used eight parameter values between 0.05 and 1.0. The consequences of changing *SoluteBindingProb* influenced the peak (but only slightly), the shape, and the tail end of the outflow profile. The results in Fig. 6C are for values of 0.05 and 0.999 (for LABETALOL in Fig. 4C it was 0.6). Increasing *SoluteBinding-*

Prob decreased the peak, lowered the tail end of outflow profile, and increased METABOLISM: Area Ratio=0.8. Because of the increased probability of binding in Grids B and C, fewer of the COMPOUNDS that reached Grids B and C could return quickly to Grid A and the Core. Consequently, post-peak values were lower. Increasing binding probability in Grids B and C increased the residence time in those spaces, increasing METABOLISM. Decreasing *SoluteBindingProb* to 0.05 had the opposite effects: peak height increased, profile shape changed, and the tail end of the profile was raised: Area Ratio=2.2.

Eight *MetabolizeProb* parameter values were studied. The consequences of change (Fig. 6D) were essentially the same as changing *B2CJumpProb*. When the value was increased to 0.95 (from 0.3 for LABETALOL in Fig. 4C), the tail end of the outflow profile was lowered and METABOLISM increased: Area Ratio=0.88. Because the change only influenced COMPOUNDS that had already reached Grid C and were within the HEPATOCYTES, the outflow profile's peak was not significantly influenced. When *MetabolizeProb* decreased to 0.05, the consequences were opposite those just described: Area Ratio=1.3.
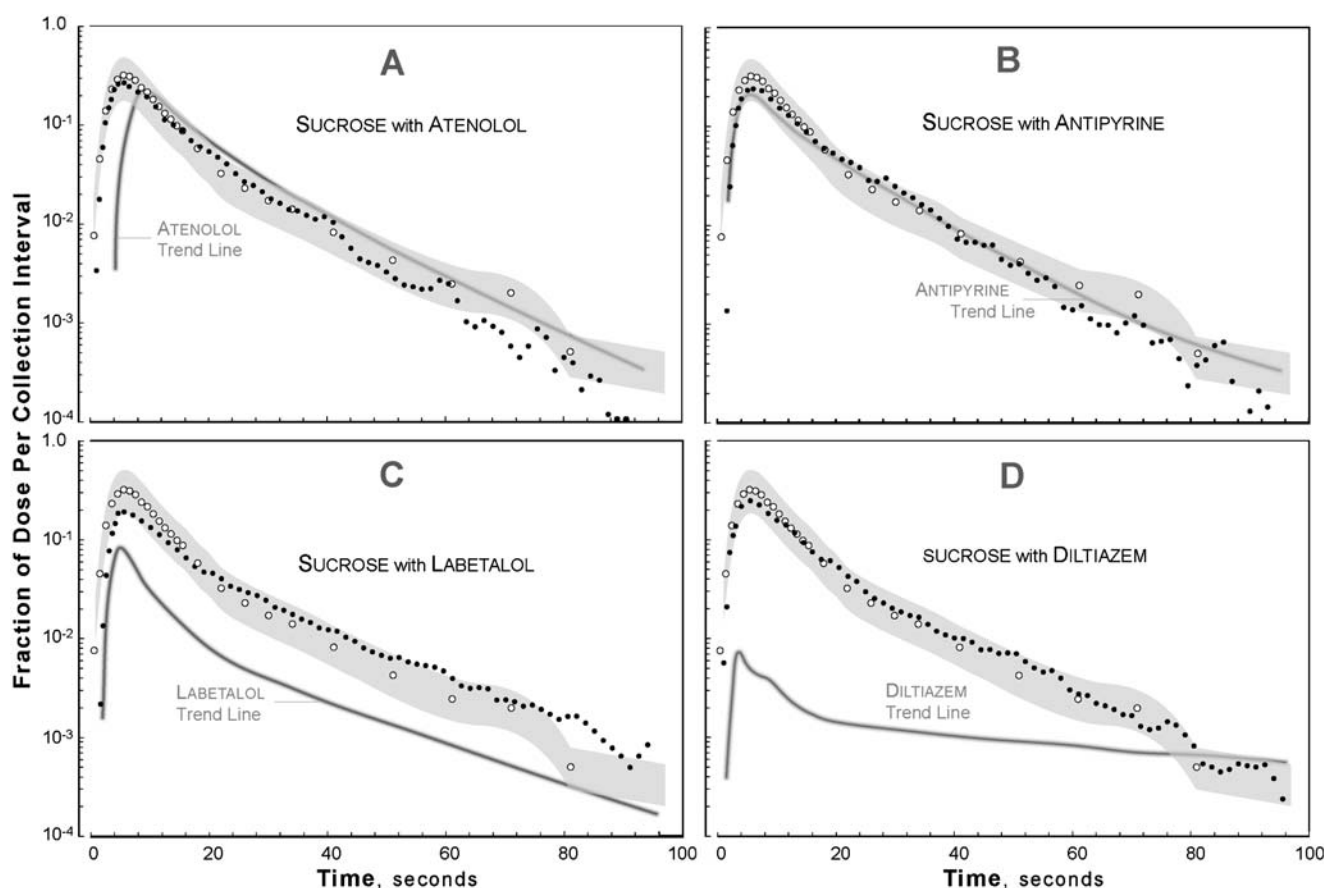
Fig. 5. Semilog plots of outflow data for SUCROSE when co-administrated with each DRUG in Fig. 4. *Open circles* Mean wet-lab outflow values for sucrose. The *gray band* represents the mean±one standard deviation for the referent wet-lab sucrose data. The *gray curve* is the DRUG trend line from Fig. 4.

Visualization of Simulation Details

Because of the design and discretized features of the ISL, the details of events as COMPOUNDS trek through various SS can be easily visualized for experimental, verification, and/or validation purposes. An interactive movie of SUCROSE and ATENOLOL moving separately through the ISL following a single combined dose is provided within Supplementary Material ESM.

DISCUSSION

ISLs and Traditional Models

The stated objective of this work was to instantiate a physiologically and mechanistically realistic software device, which could be used and reused to simulate hepatic outflow profiles of any of five compounds, alone or in combination, and study plausible, detailed, generative mechanisms. The results (Figs. 4, 5 and 6) provide the validation evidence that the objective has been achieved. The physiological and mechanistic realism of the ISL derives in part from component design and connectivity, and from how mobile components—representing drugs of interest—interact with spatially fixed components. Static and dynamic relationships within the ISL, although currently abstract and low resolution, are intended to map to corresponding relationships within a liver

during perfusion. In that sense, the ISL is physiologically and mechanistically realistic, although it uses parameters and values different from traditional, continuous, physiologically-based models.

It should be emphasized that Hung *et al.* (5) used a two-phase stochastic, PBPK model and nonlinear regression to fit the referent data in Figs. 4 and 5. The authors state, "this model perfectly fitted the data from the peak to the tail." ISL outflow profiles have provided a description of the original experimental data that is inferior to that obtained by the parsimonious nonlinear regression approach. However, it is evident that ISL simulations, as previously detailed (2), are better placed to meet the constructive goal of describing the causes of PK phenomena, predicting how detailed changes in the system affect those phenomena, and that ISL simulations yield profiles that are fairly similar to those obtained by regression.

The amount of detail included in this version of the ISL is purposefully just enough to represent the outflow profiles of the four drugs and sucrose. For example, the current coarse-grained movement of COMPOUND is modeled differently within and between grids than within CELLS, and can be refined differently for each space when that is needed. For example, we could replace the two probabilities for jumping between Grids A and B with specific details. No transporters were specifically represented, even though we know several varieties exist. They, along with other cellular
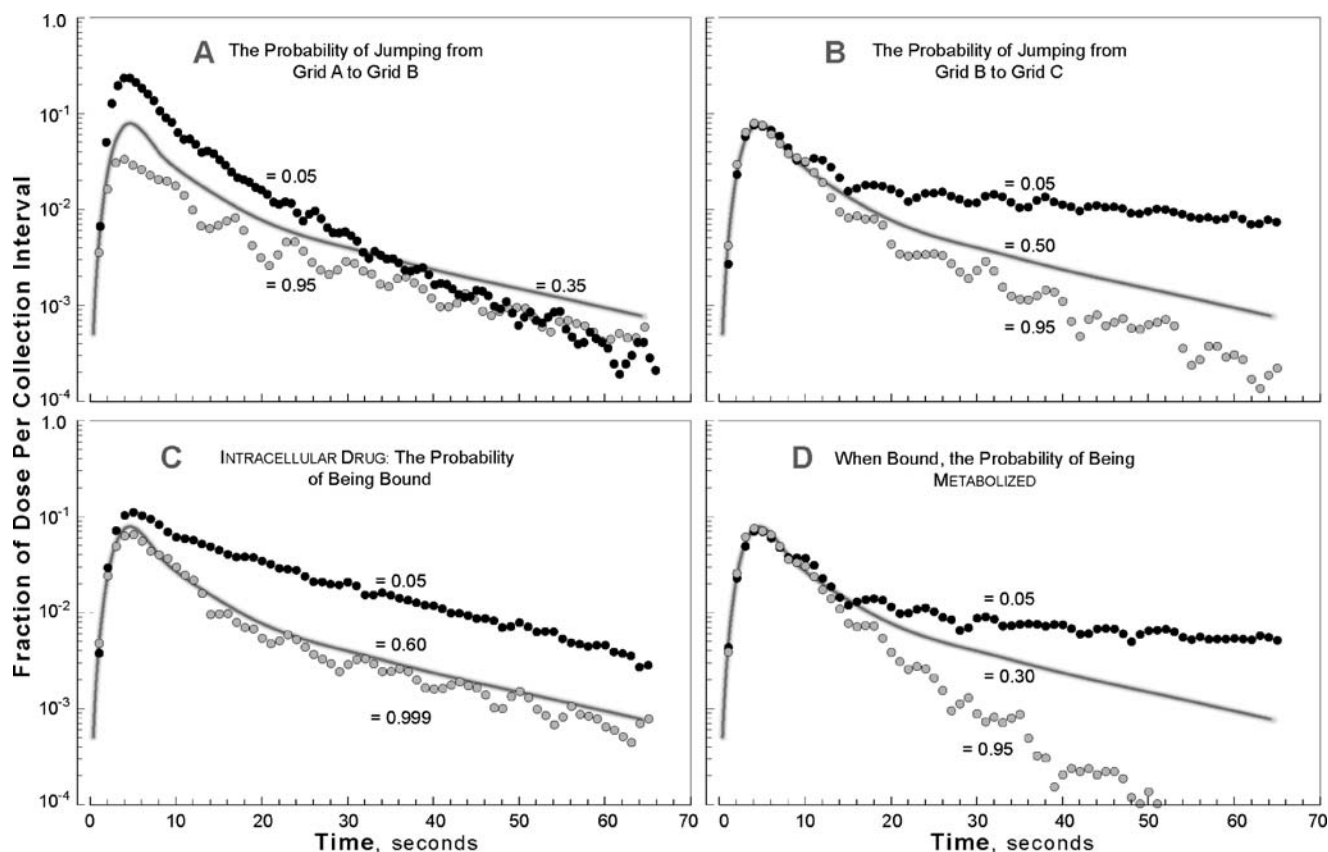
Fig. 6. Semilog plots demonstrating the consequences of changing four parameter values. In each graph, the continuous gray curve is the trend line for the LABETALOL data in Fig. 4C, and it provides reference to which the experimental values should be compared. Experiments: LABETALOL and SUCROSE were administered as for Fig. 4C; however, one parameter value (indicated) was either increased or decreased relative to the control value for LABETALOL (shown). Only LABETALOL data are shown because these parameter values are DRUG-specific and do not influence the behavior of co-administered SUCROSE. The parameter values changed determine the probability of one of four events occurring within any one simulation cycle: **A** jumping from Grid A to B (parameter: *A2BJumpProb*); **B** jumping from Grid B to C (parameter: *B2CJumpProb*); **C** being bound by a binder (parameter: *SoluteBindingProb*); and **D** being metabolized when bound (parameter: *MetabolizeProb*).

material, have been conflated into the abstract binder objects. We can implement a spatially detailed CELL MEMBRANE, as done in (17), and imbue it with transporter objects, as done in (18). A random walk mechanism for DRUG transport was adequate to simulate the referent disposition behaviors. More complicated transport phenomena can be added, without compromising the functionality already present when model use requires doing so.

It is too early to make claims about the relative predictive strengths of the ISL class and classical PBPK models. For that, the ISL will need to be challenged to make predictions for new drugs or make predictions of disposition events from experiments that use experimental designs different from that used for validation. Nevertheless, it is important to note that the ISL has been carefully designed specifically to meet such challenges. It has been designed to exhibit ten capabilities (see Supplementary Material) and the results demonstrate that the ISL exhibits nine of the ten. The following are the five that are most relevant to future use of ISLs for prediction.

– It must be easy to *reconfigure* an ISL to represent different histological, physiological, or experimental conditions.
– In order to represent the particular specifics of different experiments, it must be relatively simple to change ISL

usage and assumptions, or increase or decrease detail, without requiring significant re-engineering.
– To facilitate the two preceding capabilities, it must be easy to join, disconnect, and replace ISL components: ISL components *articulate*. It must be straightforward to separately validate components. This capability was also demonstrated in (17) and (18).
– The ISL must be usable for simulating the disposition, clearance, and metabolic properties of a wide variety of *compounds*, separately or in the same experiment.
– It must be easy to use a validated ISL as an organ component within a larger, synthetic, physiologically based, whole organism model (not yet demonstrated).

All computational models designed to exhibit the same behavior are effectively identical. However, different models often have different goals, which manifest in differences between components, their organization, and their implementation. For instance, the classical, inductive PBPK models exemplified in (3–8) make parsimony paramount in order to insure identifiably and minimize parameter uncertainty. Such models seek to faithfully describe the time course of PK data in terms of physiological events occurring globally within the liver. Both an advantage and a limitation is that, as a top down approach providing that global view of events, they

must ignore intricacies and system heterogeneity. Hence, classical PK models are the best option for precisely describing the global behavior of the system using a mathematically minimal representation. In contrast, the ISL works locally, middle-out, in providing a description of the articulation of hepatic components. For the task of representing PK data appropriately using minimalist models, the ISL and their ilk will be inferior to classical PBPK models.

The ISL's real power is experimental exploration of what biochemical, morphological, and physiological alterations in subcellular and local mechanisms may have on PK phenomena. In (2) we demonstrated the consequences of simulated lobular morphological and physiological changes. The outflow profile changes in Fig. 6 show results from event changes within each SS. The different profiles could represent the consequence of disposition of the same drug in a different liver in which changes in subcellular and local mechanisms are caused by biochemical, morphological, and physiological alterations. Alternatively, the different profiles could be caused by changes in subcellular and local mechanistic details that are a consequence of dosing with a different drug. In the latter case, the specific ISL parameter change, the probability of jumping from Grid B to Grid C, for example, may be traceable to differences in a specific subset of PCPs. Hence, if the goal is to predict altered PK caused by altered pathophysiology or a change in drug structure, or to discover why liver disease leads to a particular PK phenomena rather than another, then the ISL class is likely to be among the best options. Further, if the researcher intends to also use a model to explore the PK consequences of specific mechanistic changes that may result, for example, from disease or co-administered drugs, then models of the ISL class are expected to have advantages. However, at this time, the ISL class has not been used for such purposes and so we must await the supporting evidence. The discussions of comparisons of inductive PBPK models and synthetic models of the ISL class in (2) (including Supplementary Material) and (9,10,19,20) address other ways that the ISL class differs from traditional PBPK models.

Disposition Mechanisms

Features of hepatic architecture at several levels of detail are encountered by all xenobiotics traveling through the liver. Our approach (Figs. 1 and 2) has been to represent some of those common features within Sinusoidal Segments. Probabilistic parameters control how each spatially fixed component interacts with mobile objects representing drugs, and these interactions can be tailored to the PCPs of different compounds. Fixed ISL components "read" PCP information carried by each COMPOUND before initiating an interaction. Consequently, several different DRUGS can be present during the same simulation. SUCROSE plus the four DRUGS can be administered together and the outflow profile of each will be experimentally indistinguishable from referent profiles.

The mechanisms within the ISL are relevant for other drug classes because the rules governing interaction between a mobile object and a fixed component can range from nil to extreme. Sheihk-Bahaei *et al.* (18) have provided an example of applying exactly the same methods to two very different compounds: salicylate and enkephalin; in (11) the study was

extended to include taurocholate and methotrexate. They tuned in silico hepatocytes to simulate the uptake and biliary clearance of those four compounds in sandwich-cultured hepatocytes. Metabolic enzymes and transporters are specifically represented. It is at this level of detail that CYP enzyme and transporter polymorphisms could be represented within an ISL, where separate enzyme and/or ISL versions simulate a specific polymorph.

With additional ISL validations comes the opportunity to anticipate or predict ISL parameter values for a new compound, based on its PCPs. There is a mapping between the space of ISL parameterizations and the space of compounds' PCPs. The expectation is that as the number of satisfactorily validated COMPOUNDS increases, identifiable patterns will emerge in these mappings. In that situation, the ISL can be given methods to exploit and use posited mappings to anticipate a reasonable set of parameter values for a new, previously unseen DRUG, given only its PCPs. An example of how this can be done was recently presented (11).

The conceptual separation of hepatic form and function and their subsequent instantiation within the ISL has been somewhat arbitrary. For example, extracellular access to Grid C is regulated by the density of FENESTRATIONS within Grid B combined with the probability of jumping to Grid C when a FENESTRATION is encountered. A set of different FENESTRATION densities and transition probabilities values may give the same Grid C access for a given COMPOUND. This example illustrates that different interactions between LOBULE structural components and mobile COMPOUNDS of the same type can similarly impact disposition within the ISL. Sets similar to the preceding example exist for each probabilistic parameter influenced by PCPs. Importantly, the size of these sets shrinks when the same ISL is also validated sequentially against data for a second compound. It shrinks further for each additional, successful validation.

Tuning and Refining ISLs

The iterative model refinement method is the heart of exploratory modeling. When faced with the task of building a scientifically relevant model in the face of significant gaps in the body of knowledge used to guide the modeling, parameterizations and model components must strike a flexible balance between too many and too few. Too many can imply redundancy or a lack of generality; too few can make the model useless for practical research. With the ISL, we have attempted to create a minimal model, both abstract enough to be meaningful and concrete enough to provide a foundation from which future ISL descendents can develop. As the ISL evolves, we expect to refine the above, compensatory parameter sets such that they guide further experimentation on the model and the referent. For current use, the ISL is striking that balance between too many and too few components and parameters.

The structural and microarchitectural details for each simulation are nondeterministic. Graph structure has a major influence on ISL outflow profiles (2). Even though the number of nodes per zone and the number of intra- and interzone edges are specified, the connectivity pattern is determined randomly at the start of each simulation. SS structures for a given set of parameter values are also

stochastic: the actual structures of the 72 SSs used for each ISL run in Figs. 4 and 5 are highly constrained yet typically different, and their properties can form clusters as a consequence of the discretization within an ISL. Because of the many forms of discretization, there is variability between ISL instantiations and that causes outflow profiles to be somewhat different. That variability reflects, and to some extent simulates, some of the uncertainty in our knowledge about the exact details of the generative mechanisms and wet-lab experiments from which the data were collected.

Each 48-trial experiment models a single rat liver. Two experiments using the same parameter vector are unlikely to vary enough to represent two different individuals. Instead, they effectively simulate repeat experiments on a single liver where, unlike with the referent livers, hepatic function is not modified by a previous experiment. To effectively simulate interindividual variances, some modification of the parameter vector is needed. For variance in liver size and blood flow, we can modify *CoreFlowRate*, the number of SSs, the geometry of the SSs, and *SinusoidTurbo*. HEPATOCYTE and ENDOTHELIAL CELL density, binder, and METABOLISM parameters can be changed to vary the overall amount of HEPATIC function and that can simulate interindividual differences in age, damage to the liver, or previous exposure to compounds that induce enzymes. Various types of liver damage can also be simulated by changing the ratio between the two types of SS or by making the SSs more or less constricted and tortuous. The connectivity of the SS graph can also be changed to increase or decrease intra-LOBULE mixing, or increase or decrease the range of possible path lengths.

We do not measure or record frequencies of path "lengths" or path properties encountered by COMPOUNDS as they move from PV to CV. If we could obtain such data during liver perfusions, we might expect a smooth and asymmetric distribution ranging from short to long treks (6). In the ISL, if the treks taken by COMPOUNDS form clusters, then the outflow profile will provide evidence that heterogeneity by exhibiting post-peak bumps in the outflow profile like those seen in Fig. 6. Such patterns are a natural consequence of how we discretized the ISL. For example, decreasing the probability of moving from Grid A to B (Fig. 6A) reduces COMPOUND resident time within Grids B and C. The bumpy tail of the outflow profile reflects primarily that, when COMPOUNDS are confined more to Grid A and the Core, the available path options from PV to CV are reduced, and the frequency distribution of paths taken becomes less smooth (data not shown). Having more options smoothes the curve; decreasing the probability of moving from Grid A to B reduces options. Similarly, setting the probability of moving from Grid B to C (Fig. 6B) to a high value increases the fraction of resident time spent by COMPOUNDS within Grid C. The lowered, bumpy tail is a consequence of reduced path options: the frequency distribution of paths taken from PV to CV became somewhat clustered because options were reduced.

The experimental outflow profiles in Fig. 6B and D show that two different mechanistic changes can cause similarly altered outflow profiles. Consequently, differences between two outflow profiles, as discussed above, can have multiple, equally valid, detailed explanations. We speculate that the same is true *in situ* and *in vivo*.

In "MATERIALS AND METHODS", we stated that BINDERS are INTRACELLULAR components that collectively represent transporters, enzymes, organelles, and other cellular components that bind or sequester drug molecules. DILTIAZEM "sees" more BINDERS than do the other three DRUGS. As mentioned in RESULTS, the probability of a bound DILTIAZEM being METABOLIZED within a simulation cycle is very small: 0.02. That value may initially seem inconsistent with reports that diltiazem has a large, relative, intrinsic hepatic clearance. However, by positing that a large portion of DILTIAZEM binding within the ISL maps to intracellular ion-trapping and microsomal binding, we see that the ISL mechanisms and event parameterizations for DILTIAZEM, although less specific and more abstract, are completely consistent with mechanistic ideas that motivated traditional PK models (5,8). We could replace BINDERS with two (or more) new INTRACELLULAR object classes, one representing intracellular ion-trapping and microsomal binding, and another representing drug metabolism. However, because current model use did not require that detail, we elected not to do so.

Designed ISL Capabilities

We have demonstrated and validated an ISL that provides new methods for achieving the PBPK vision. It proved essential that the ISL have the ten capabilities listed in Supplementary Material ESM. ISL observables have been designed to be consistent with *in situ* observables. This design has enabled clear mappings between *in vitro* and in silico components and mechanisms that can be harnessed for prediction. As *in situ*, the ISL behaviors that have emerged during simulated perfusion experiments are the consequences of local mechanisms: local component interactions. Simulation details as they unfold are visualizable, measurable, and comparable to those of *in situ* perfused livers (see Supplementary Material). The ISL has been designed and constructed so that it can become the liver component in a larger, whole organism model. To enable that adaptability and use the same ISL for several different compounds, we found it essential that components be autonomous and easily reconfigured. By making components and system dynamics discrete, it was relatively simple to increase or decrease detail as needed to simulate outflow profiles of additional COMPOUNDS, without requiring significant ISL reengineering. Because identical PK profiles can be a consequence of different mechanisms, we have made it easy to join, disconnect, and replace ISL components to explore alternate explanations.

REFERENCES

1. M. Rowland, L. Balant, and C. Peck. Physiologically based pharmacokinetics in drug development and regulatory science: a workshop report (Georgetown University, Washington, DC, May 29–30, 2002). *AAPS PharmSci* **6**:E6, 2004 (2004).
2. C. A. Hunt, G. E. Ropella, L. Yan, D. Y. Hung, and M. S. Roberts. Physiologically based synthetic models of hepatic disposition. *J. Pharmacokinet. Pharmacodyn* **33**:737–772 (2006).
3. Y. G. Anissimov and M. S. Roberts. A compartmental model of hepatic disposition kinetics: 1. Model development and application to linear kinetics. *J. Pharmacokinet. Pharmacodyn.* **29**:131–156 (2002).
4. D. Y. Hung, P. Chang, K. Cheung, B. McWhinney, P. P. Masci, M. Weiss, and M. S. Roberts. Cationic drug pharmacokinetics in diseased livers determined by fibrosis index, hepatic protein content, microsomal activity, and nature of drug. *J. Pharmacol. Exp. Ther* **301**:1079–1087 (2002).
5. D. Y. Hung, P. Chang, M. Weiss, and M. S. Roberts. Structure-hepatic disposition relationships for cationic drugs in isolated perfused rat livers: transmembrane exchange and cytoplasmic binding process. *J. Pharmacol. Exp. Ther* **297**:780–789 (2001).
6. L. Liu and K. S. Pang. An integrated approach to model hepatic drug clearance. *Eur. J. Pharm. Sci* **29**:215–230 (2006).
7. M. S. Roberts and Y. G. Anissimov. Modeling of hepatic elimination and organ distribution kinetics with the extended convection-dispersion model. *J. Pharmacokinet. Biopharm* **27**:343–382 (1999).
8. G. A. Siebert, D. Y. Hung, P. Chang, and M. S. Roberts. Ion-trapping, microsomal binding, and unbound drug distribution in the hepatic retention of basic drugs. *J. Pharmacol. Exp. Ther* **308**:228–235 (2004).
9. Y. Liu, and C. A. Hunt. Studies of intestinal drug transport using an in silico epithelio-mimetic device. *Biosystems* **82**:154–167 (2005).
10. Y. Liu and C. A. Hunt. Mechanistic study of the cellular interplay of transport and metabolism using the synthetic modeling method. *Pharm. Res* **23**:493–505 (2006).
11. S. Sheikh-Bahaei and C. A. Hunt. Prediction of *in vitro* hepatic biliary excretion using stochastic agent-based modeling and fuzzy clustering. In L. F. Perrone and *et al.* (eds.), Proceedings of the 37th conference on Winter simulation, Monterey, CA, 2006, pp. 1617–1624.
12. H. Steen, R. Oosting, and D. K. Meijer. Mechanisms for the uptake of cationic drugs by the liver: a study with tributylmethylammonium (TBuMA). *J. Pharmacol. Exp. Ther* **258**:537–543 (1991).
13. K. Cheung, P. E. Hickman, J. M. Potter, N. I. Walker, M. Jericho, R. Haslam, and M. S. Roberts. An optimized model for rat liver perfusion studies. *J. Surg. Res* **66**:81–89 (1996).
14. H. F. Teutsch, D. Schuerfeld, and E. Groezinger. Three-dimensional reconstruction of parenchymal units in the liver of the rat. *Hepatology* **29**:494–505 (1999).
15. D. L. Miller, C. S. Zanolli, and J. J. Gumucio. Quantitative morphology of the sinusoids of the hepatic acinus. Quantimet analysis of rat liver. *Gastroenterology* **76**:965–969 (1979).
16. J. J. Gumucio and D. L. Miller. Zonal hepatic function: solute-hepatocyte interactions within the liver acinus. *Prog. Liver Dis* **7**:17–30 (1982).
17. L. X. Garmire, D. G. Garmire, and C. A. Hunt. An in silico transwell device for the study of drug transport and drug–drug interactions. *Pharm Res* **24**:2171–2186.
18. S. Sheikh-Bahaei, G. E. P. Ropella, and C. A. Hunt. In silico hepatocyte: agent-based modeling of the biliary excretion of drugs *in vitro*. In L. Yilmaz *et al* (eds.), *Proceedings of the Agent-Directed Simulation Symposium of the Spring Simulation Multiconference (SMC'06)*, SCS Press, San Diego, CA, 2006, pp. 157–163.
19. G. E. Ropella, C. A. Hunt, and D. A. Nag. Using heuristic models to bridge the gap between analytic and experimental models in biology. In L. Yilmaz (ed), Proc 2005 Agent-Direc Simul Symp (ADS'05), Simulation Series, Vol. 37, SCS Press, San Diego, CA, 2005, pp. 182–190.
20. G. E. Ropella, C. A. Hunt, and S. Sheikh-Bahaei. Methodological Considerations of Heuristic Modeling of Biological Systems, Proc 9th World Multi-Conf Systemics, Cybernetics and Informatics, Orlando, Florida, 2005.